SCIENTIFIC PAPER
Published: June 12, 2026
https://doi.org/10.13167/2026.32.11

An approach to pullout resistance determination for wrap-around geotextiles in flood embankments

Željko Šreng[1]✉, Luka Juretić[1], Krunoslav Minažek[1] and Goran Lončar[2]

[1] *Josip Juraj Strossmayer University of Osijek, Faculty of Civil Engineering and Architecture Osijek, Vladimir Prelog St. 3, 31000, Osijek, Croatia*

[2] *University of Zagreb, Faculty of Civil Engineering, Fra Andrije Kačića-Miošića 26, 10 000 Zagreb, Croatia*

Corresponding author:
Željko Šreng

Received:
October 1, 2025

Revised:
February 16, 2026

Accepted:
March 26, 2026

Published:
June 12, 2026

Citation:
Šreng, Ž. et al.
An approach to pullout resistance determination for wrap-around geotextiles in flood embankments.
Advances in Civil and Architectural Engineering,
2026, 17 (32), pp. 189-204.
https://doi.org/10.13167/2026.32.11

ADVANCES IN CIVIL AND ARCHITECTURAL ENGINEERING (ISSN 2975-3848)

Faculty of Civil Engineering and Architecture Osijek
Josip Juraj Strossmayer University of Osijek
Vladimira Preloga 3
31000 Osijek
CROATIA

Abstract:
This study proposes an alternative verification procedure for assessing the pullout resistance of wrap-around geotextiles in flood embankments. The research does not aim to determine the design pullout resistance for practical engineering applications directly, but rather, to evaluate the geotextile pullout force within small-scale physical models intended for conceptual-level analysis. The approach addresses the limitations of standard numerical models in capturing the actual slope failure mechanism. It also accounts for the stabilising effect of geotextile wrapping, which is often insufficiently represented in conventional analyses. The proposed approach integrates physical experiments with analytical and numerical modelling. Small-scale embankment models subjected to seepage-induced hydraulic and slope stability failure were reinforced with wrap-around geotextiles of varying anchorage lengths and wrap-around heights along the downstream toe. The observed stability or failure of the physical models was used to evaluate the analytical formulation. The analytical model is based on a comparative calculation of hydrodynamic force and geotextile pullout force. The analytically derived pullout force was implemented in GeoStudio:SLOPE/W to assess the embankment stability. A comparative assessment of the physical, analytical, and numerical results showed good agreement, confirming the reliability of the proposed verification approach. The developed analytical model, validated through numerical simulations and experimental observations, represents a useful tool for the conceptual evaluation of embankment stability mechanisms.

Keywords:
analytical model; embankment; geotextile; numerical simulation; physical experiment; slope stability

1 Introduction

The loss of stability in embankments most often occurs because of uncontrolled seepage, excessive pore pressures, and a reduction in the effective stresses, which consequently lead to liquefaction as well as internal and external erosion of the fill material. Therefore, the application of modern solutions such as geosynthetics is of great importance, because they directly contribute to the safety, durability, and reliability of embankments throughout their design period [1]. Geosynthetics have been used in engineering practice for over 60 years for the construction and rehabilitation of earthfill structures. Their applicability has been steadily increasing because of their wide range of functionalities and proven reliability [2]. Geotextiles, as a type of geosynthetics, provide multiple functions including filtration, drainage, separation, reinforcement, and protection. Their use enables the application of locally available soils with poorer geotechnical properties. The role of geotextiles in improving embankment stability is reflected in their tensile reinforcement functions and drainage capacities. Consequently, they reduce pore water pressure, thereby lowering the risk of slip surface formation [2; 3]. Typical geotextile types include nonwoven, woven, and knitted products, which are most often manufactured from polymers such as polypropylene, polyester, polyethylene, and polyamide. Their effectiveness depends on the mechanical properties, soil–geotextile interactions, and proper installation, necessitating precise modelling and empirical validation [1; 4]. Consequently, both the literature and engineering practice emphasise the importance of combined approaches, in which physical modelling is used to observe real structural behaviour while numerical and analytical methods support the interpretation and generalisation of results [5].

Previous studies have shown that geotextiles with a sufficient anchorage length and wrap height can significantly enhance embankment stability [6-9]. In contrast, inadequately dimensioned or improperly installed geotextiles cannot effectively prevent shear failure [3; 10]. The position and length of the reinforcement layers play a decisive role in determining the factor of safety against sliding and in shifting potential slip surfaces toward the upper soil layers [3; 5]. Thuo et al. [11] demonstrated that the strategic placement of geotextile layers can prevent pore pressure development at the base of embankments, highlighting the importance of proper installation for stability. Arsyad [12] emphasised the need to adjust the number of geotextile layers according to stability analyses for each specific embankment to achieve optimal reinforcement. Rahman and Lee [13] conducted a parametric study on geotextile-reinforced soil stability by considering the tensile stiffness as well as the number and length of reinforcement layers within embankments. Zimbu et al. [14] evaluated the performance of reinforced embankments under different conditions and demonstrated the effect of geotextile inclination on stability. Hourani et al. [15] carried out finite element modelling of embankments on soft clay and showed that a single layer of geotextile reinforcement placed at the base could increase the factor of safety by up to 40 %.

This study represents an integrated analysis of the influence of geotextiles on the stability of model embankments by combining physical experiments with analytical and numerical approaches. Through a simplified analytical model, the purpose is to determine the relationship between the hydrodynamic force and geotextile pullout resistance. The obtained pullout force is then introduced as an input parameter in the numerical stability analyses to represent the additional resistance provided by the geotextile. The analytical formulation of the hydrodynamic action is based on the fundamental laws of fluid mechanics (conservation of mass and momentum) applied to a defined control volume. This approach is not commonly used in conventional geotechnical stability analyses, in which soil strength parameters and limit equilibrium formulations are typically employed. However, the coupled seepage–stability problem is inherently complex, particularly at a small scale where soil strength parameters are difficult to define with confidence and realistic slip surface geometries are difficult to prescribe. Therefore, the hydrodynamics-based formulation adopted in this study is used as a simplified alternative tool for estimating the driving action leading to geotextile pullout. Thus, the method

is not proposed as a direct design procedure but as an alternative means for assessing stability conditions in a controlled experimental framework.

2 Methodology

Standard numerical slope stability models primarily assess the global stability and represent geotextiles as axial tensile elements. Such a representation is generally adequate for global limit equilibrium analyses; however, it does not explicitly reproduce local failure mechanisms at the downstream toe, where the combined hydraulic action and soil–geotextile interactions govern the onset of instability. Numerical models have a limited capability to simulate the pullout of wrap-around geotextiles and the associated local loss of stability at the downstream toe (Figure 1). To address this limitation, this study focuses on local rather than global embankment stability and proposes an alternative methodology for evaluating the stabilising effect of wrap-around geotextiles.

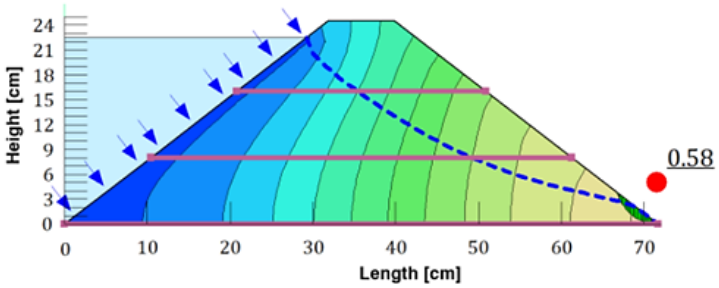

Figure 1. Example of the inability of numerical analysis to capture local soil failure [9]

2.1 Methodology

The methodology was based on physical experiments and analytical modelling of seepage and embankment stability, with the observed phenomena and derived equations subsequently applied within a numerical model (Figure 2). The first step involved conducting physical experiments on embankment models in the laboratory of the Faculty of Civil Engineering and Architecture Osijek. The experiments differed in terms of the anchorage length Lan of the geotextiles embedded in the model and wrap-around height h_{an} of the geotextiles placed along the downstream slope. The upstream water level and overall dimensions of the model remained constant across all of the experiments. The physical experiments provided insights into the local stability at the downstream toe and the mechanisms of failure, where failures occurred.

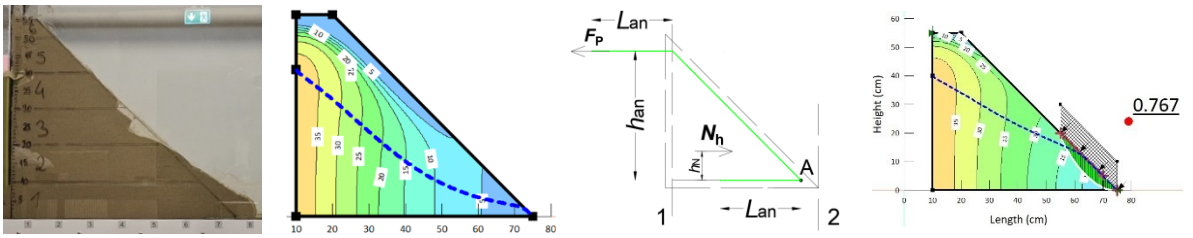

1. Physical experiment (failure mechanism)
2. Seepage analysis (seepage flow and velocities)
3. Analytical model (pullout force, moment M_A, failure evaluation)
4. Numerical model (Failure evaluation, model validation, factor of safety)

Figure 2. Methodology steps (the expected outcomes of each step are provided in parentheses)

The analytical model was based on a comparative calculation of the geotextile pullout force F_P and acting hydrodynamic force N_H. As an initial step in the analytical stability model, seepage

through the embankment body was analysed to determine the hydrodynamic force. The hydrodynamic force was evaluated using a combination of the analytical phreatic line solution, which provided the discharge, and the numerical seepage model, from which the flow velocities were obtained. The observations from the experiments were used to develop and calibrate the analytical stability model. In this manner, the anchorage length Lan required for a given wrap-around height h_{an} to ensure local stability at the downstream toe was estimated. The analytically determined pullout force F_P was subsequently introduced into the numerical stability model to represent the effect of the geotextile inclusion.

2.2 Physical experiments

The seepage and slope stability of the homogeneous sand embankment models were analysed using an HM 169 apparatus [16]. The HM 169 device was employed for the visualisation and analysis of two-dimensional water flow through porous media and groundwater flow as well as to examine the effects of water forces on structures. To construct the models, locally available material from the downstream reaches of the Drava River was selected. The grain-size distribution of the sand was determined by sieve analysis, in accordance with HRN EN 933-1:2012. The material was classified as uniformly graded, with 97 % of the particles ranging from 0,125 to 0,500 mm. A modified Proctor test established an optimal moisture content of 7 %, which was added to the material prior to compaction [9].
To prevent slope failure and the internal erosion of soil particles, a nonwoven polypropylene geotextile with a unit mass of 80 g/m² was used. According to the technical characteristics typical for this class of materials, its thickness ranges from 0,6 to 0,9 mm, classifying it as a very thin and flexible geosynthetic, with a tensile strength of approximately 2,5 kN/m [1].
Seven homogeneous sand models with identical geometries were constructed. The upstream slope was omitted owing to space limitations of the HM 169 apparatus. The dimensions of the models and their material characteristics are listed in Table 1. The models were constructed by compacting the sand into five layers, each 10 cm thick, with a final top layer thickness of 5 cm. Compaction was performed using a wooden rammer with dimensions of 10,5 × 10,0 cm, applying a total of 10 hits per layer with a rubber mallet (five in one direction and five in the perpendicular direction).

Table 1. Basic parameters of laboratory embankment models

Parameter	Value
Dry unit weight of material γ_d [kN/m^3]	16,00
Saturated unit weight of material γ_{sat} [kN/m^3]	20,20
Crest length [cm]	10,00
Base length [cm]	65,00
Model height [cm]	55,00
Slope angle [°]	45,00
Average dry density of model ρ_d [kg/m^3]	1594,41
Mass of material used for construction [kg]	34,20
Embankment volume [cm^3]	21450,00
Upstream water height [cm]	40,00

The geotextile was used in all experiments except Experiment 1, which focused on seepage analysis and modelling. Experiments 2 to 7 differed in terms of the geotextile dimensions. In Experiments 2, 3, and 6, only the first slope layer was reinforced with geotextile (h_{an} = 10 cm), whereas in Experiments 4, 5, and 7, both the first and second layers were reinforced (h_{an} = 20 cm). Table 2 presents a complete list of the experiments conducted, indicating their roles in the analysis (calibration of seepage parameters, calibration of soil mechanical properties and analytical model parameters, and validation of calibrated parameters). Table 2 also specifies

the geotextile wrap-around height (h_{an}) and anchorage length (L_{an}) for each experiment, along with a schematic of the physical model.

Table 2. Physical experiments used to create the analytical model

Experiment	Geotextile	Function	h_{an} / L_{an} (cm)	Scheme
1	No	Calibration	-	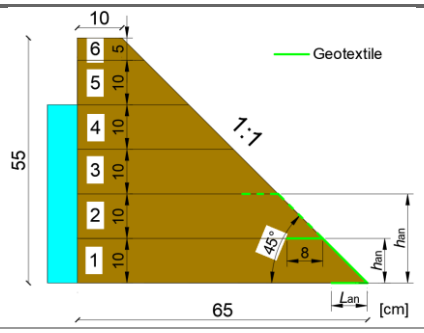
2	Yes	Calibration	10 / 4	
3	Yes	Calibration	10 / 6	
4	Yes	Calibration	20 / 8	
5	Yes	Calibration	20 / 14	
6	Yes	Validation	10 / 8	
7	Yes	Validation	20 / 12	

2.3 Analytical model

The analytical model was based on the calculation of two forces acting at the interface between the geotextile and embankment model. These are the hydrodynamic force N_H, which represents the destabilising action, and the pullout force F_P, which represents the frictional resistance acting as a stabilising force. Figure 3 shows the calculation scheme and the control volume for which the stability of the model was evaluated. The comparison of N_H and F_P was subsequently expressed through the moment of equilibrium about Point A. The analytical model was calibrated against the results of the physical experiments to ensure that the ratio of the calculated forces corresponded to the observed experimental outcome (failure or stability).

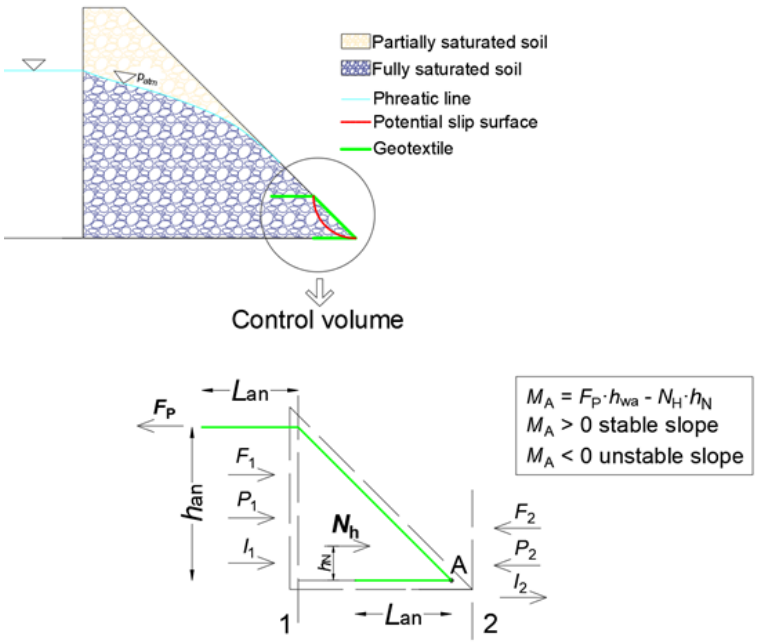

Figure 3. Control volume and scheme for calculation of hydrodynamic force N_H and moment M_A

A stability assessment was performed using an analogy from structural mechanics. The system can be idealised as an inclined beam subjected to two pullout forces F_P acting at its ends, counteracting the hydrodynamic force N_H. Based on the failure mechanism observed in

the physical models, in which no pullout of the lower geotextile was detected, an appropriate calculation scheme was adopted. Thus, the lower point (Point A) could be considered as a fixed support that acts as the centre of rotation of the system. Consequently, the stability was evaluated based on the condition of moment equilibrium about this point.
The analytical calculations were performed for all experiments listed in Table 2, except for Experiment 1, in which no geotextiles were installed.

2.3.1 Hydrodynamic force N_H

The hydrodynamic force NH was calculated using the law of conservation of momentum (Eqs. (1) to (3)). Because the water flow was predominantly in the horizontal direction, the weight component of the saturated soil within the control volume was neglected in the calculation.

$$\frac{\partial G}{\partial t} = P_1 + F_1 - P_2 - F_2 - R \tag{1}$$

$$\frac{\partial G}{\partial t} = I_2 - I_1 \tag{2}$$

$$R = N_{\mathrm{H}} = P_1 + F_1 - P_2 - F_2 + I_1 - I_2 \tag{3}$$

where $\delta G/\delta t$ represents the rate of change of momentum with respect to time, P_1 and P_2 are the hydrostatic pressure force at the inlet and outlet sections, respectively, F_1 and F_2 are the effective soil forces at the inlet and outlet sections, respectively, I_1 and I_2 are the momentum flow force at the inlet and outlet sections, respectively, and R is the reaction force, which is equal in magnitude to the hydrodynamic force N_H.
The volumetric flow rate Q was determined using Casagrande's graphical method. The seepage velocity v_2 at the outlet section of the control volume was obtained from Numerical Model 1, developed using the SEEP/W software. The effective soil forces F_1 and F_2 were calculated as follows:

$$F_{\mathrm{i}} = p_{\mathrm{t}} \cdot A = \frac{p_{\mathrm{t}} \cdot h_{\mathrm{i}}}{2} \tag{4}$$

$$p_{\mathrm{t}} = (\gamma_{\mathrm{sat}} - \gamma_{\mathrm{w}}) \cdot h_{\mathrm{i}} \cdot K_{\mathrm{t}} \tag{5}$$

where F_i is the effective soil force, which increases linearly with the depth, p_t is the soil pressure, A is the area on which the pressure acts, h_i is the height of the considered section (in this case, the difference between the upper and lower anchorage levels), and K_t is the soil pressure coefficient (determined through the calibration procedure).

2.3.2 Pullout force F_P

The pullout force F_P represents the resisting force opposing the hydrodynamic force N_H, ensuring the stability of the embankment model. The magnitude of the pullout force F_P is influenced by several factors, that is, mechanisms that occur at the interface between the geotextile and embankment body. The pullout force F_P represents the frictional resistance mobilised between the geotextile and soil along the embedded section [17]:

$$F_{\mathrm{P}} = 2 \int_0^L \sigma_{\mathrm{v}} dl \cdot L \cdot b \cdot tan\delta \tag{6}$$

where σ_v is the vertical stress along the anchorage length [N/m²], L is the anchorage length of the geotextile [m], b is the anchorage width (limited by the model width; in this case, 10,4 cm), $tan\delta$ is the tangent of the interface friction angle between the geotextile and soil, and the factor 2 accounts for the two contact surfaces between the geotextile and embankment material.
A linear distribution of the vertical stresses was assumed along the anchorage length L_{an}. The average vertical stress along the anchorage was used in the calculation of the pullout force, as follows:

$$\int_0^L \sigma_v = \overline{\sigma_v} = \frac{1}{2}\sigma_{v,max} = \frac{1}{2}\gamma_{sat} \cdot h \quad (7)$$

where $\sigma_{v,max}$ is the maximum vertical stress at the upstream edge of the geotextile, γ_{sat} is the saturated unit weight of the soil, and h is the maximum vertical distance between the geotextile and downstream slope of the model.

2.4 Numerical modelling

The numerical analysis comprised two steps: 1. Seepage analysis was performed to define the phreatic line, flow rate, velocities, pore pressures, and exit gradient under transient flow conditions (to replicate the experimental setup). 2. Slope stability analysis was performed using Spencer's method to determine the critical slip surface and factor of safety. The Spencer method considers all interslice forces and satisfies both the force and moment equilibria with the solution obtained through an iterative procedure. This method is applicable to both circular and non-circular slip surfaces. For the numerical model, a global element size of 1 cm was adopted, which resulted in a mesh comprising 2192 nodes and 2088 elements. The cell size was determined using a calibration procedure in the seepage analysis. A saturated/unsaturated model was used in this analysis because of the inherent behaviour of the embankment under seepage conditions. The boundary conditions for the transient analysis are shown in Figure 4. The geometry, boundary conditions, material properties, and duration of analysis of Numerical Model 1 served as the basis for the development of the subsequent models in which the influence of the geotextiles on the slope stability was analysed. The Entry and Exit method was used for the slip surface analysis. The entry and exit ranges were defined to correspond to the geotextile wrap-around length. The position of the exit point was based on observations from the physical experiments that identified the failure location at the toe of the downstream slope.

Because the GeoStudio software models geotextiles exclusively as tensile forces, which is insufficient to simulate the wrap-around effect (slope protection lining), their influence was represented by applying a continuous load. This load was defined using the surcharge load option, applied either in the vertical direction or normal to the ground surface [9; 18].

The unit weight of the continuous load (γ_S) was defined based on the calculated pullout force F_P:

$$\gamma_s = \frac{F_p}{b \cdot h \cdot L_{wa}} \quad (8)$$

where b is the width of the experimental chamber (10,4 cm), h is the reference height (10 cm), and L_{wa} is the geotextile wrap-around length (either 14,14 or 28,28 cm).

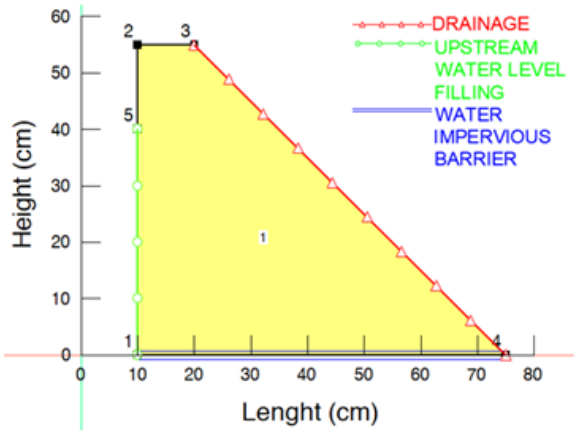

Figure 4. Boundary conditions of transient analysis

3 Results and discussion

3.1 Physical experiments

As the limits of the internal friction angle of sand (φ = 30°-45°) are less than or equal to the downstream slope angle (β = 45°), according to the Mohr–Coulomb failure criterion, a downstream slope without reinforcement is expected to be unstable (shear failure of the soil is inevitable). The results of the physical experiments are presented in Table 3. For each variant, the anchorage length L_{an} of the geotextile and wrap-around height h_{an} are indicated.

Table 3. Results of physical experiments

Experiment	Surface failure	Sliding surface	Notes
1 Without geotextile	Yes	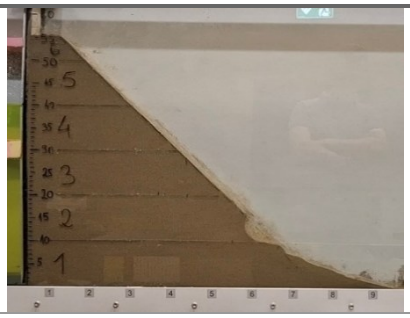	In the inlet chamber, the water reached the overflow height of 40 cm after 22 s, while the model became fully saturated after 19.5 min, with shear failure of the downstream slope initiating 99 s later.
2 h_{an} = 10 cm L_{an} = 4 cm	Yes	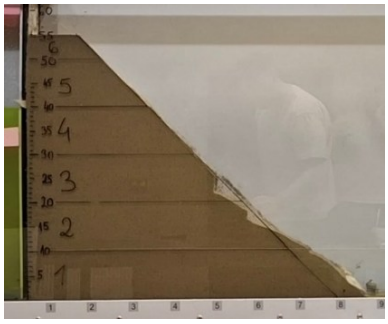	Failure of the downstream slope occurred 113 s after saturation. The slightly delayed failure can be attributed to the partial resistance of the geotextile to the hydrodynamic force. Its influence was reflected in a higher position of the phreatic line, a larger volume of saturated material, an increased zone of effective stresses, and an upward shift of the slip surface.
3 h_{an} = 10 cm L_{an} = 6 cm	Yes	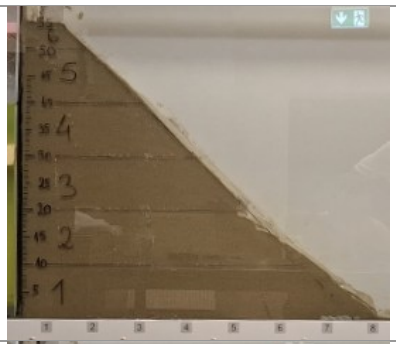	Failure occurred 220 s after saturation owing to the insufficient pullout resistance of the upper portion of the geotextile, confirming that stability depends precisely on this part. Therefore, the calibration and analysis focused on the pullout force of the upper geotextile section and its wrap-around part as the key factors of slope stability.
4 h_{an} = 20 cm L_{an} = 8 cm	Yes	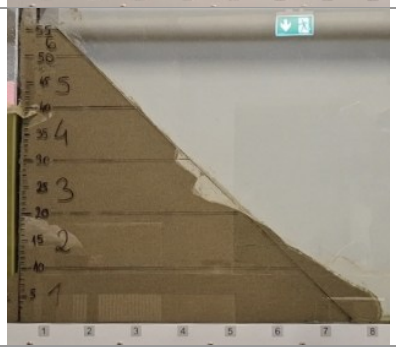	Failure occurred 148 s after saturation owing to pullout of the upper geotextile section, as in Experiment 3. The faster failure indicates the effect of a greater hydrodynamic force, which, according to the analytical model, increases with the wrap-around length.

5 h_{an} = 20 cm L_{an} = 14 cm	No	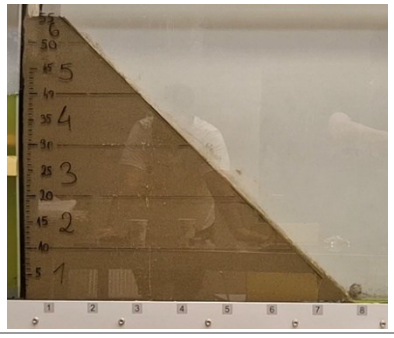	Unlike the other models, this one remained stable. An anchorage length of 14 cm was sufficient to ensure overall stability of the downstream slope. Only minor displacements of the upper geotextile were observed, accompanied by slight bulging of the wrapped portion.

3.2 Calibration of seepage model

First, the seepage model was calibrated in the numerical analysis to obtain a phreatic line identical to that observed in Experiment 1. In this way, the velocities at sections 1 and 2 (Figure 3), which were required for the calculation of the hydrodynamic force N_H, were determined. To perform the SEEP/W analysis successfully, a video recording from Experiment 1 was used. The following soil parameters were adopted through calibration to reproduce an identical progression of seepage over time:

- anisotropy with K_y/K_x = 0,9;
- volumetric water content of saturated soil Θ_{sat} = 0,32;
- compressibility m_v = 0,06 1/kPa;
- hydraulic conductivity $K_x = 5 \cdot 10^{-5}$ m/s;
- residual water content taken as 10% of the volumetric water content Θ_r = 0,032.

All calibration parameters were within the ranges of values reported in previous studies [19-22]. The volumetric water content in the saturated state Θsat corresponds to typical porosity values of compacted sand, n = 0,30-0,35 [23; 24].
The transient analysis showed that the positions of the phreatic lines over time fully coincided with those observed in Experiment 1. Figure 5 shows the phreatic line positions at the time steps t = 3, 6, and 12 min.

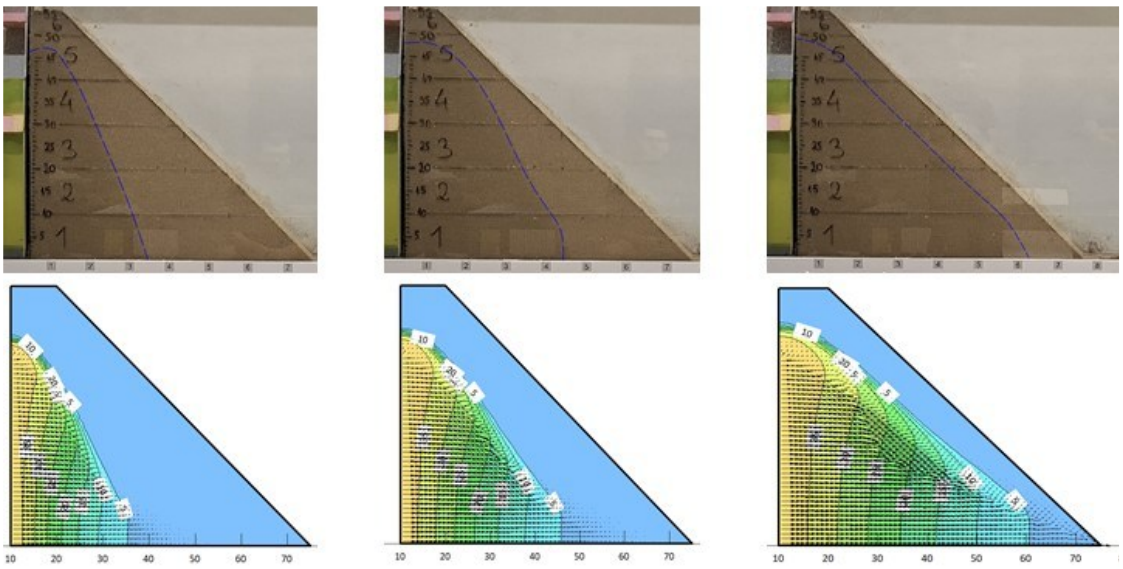

a) b) c)

Figure 5. Position of phreatic line for Model 1: a) t = 3 min; b) t = 6 min; and c) t = 12 min

The discharge, velocity, and momentum flow force values are listed in Table 4. The seepage velocity at the outlet section (v_2) remained the same regardless of the geotextile wrap-around height h_{an} and was obtained from Numerical Model 1.

Table 4. Hydromechanical characteristics of models

Parameter	h_{an} = 10 cm (Models 2, 3, and 6)	h_{an} = 20 cm (Models 4, 5, and 7)
Flow Q [m^3/s]	$5{,}89 \cdot 10^{-7}$	$5{,}89 \cdot 10^{-7}$
Velocity v_1 [m/s]	$5{,}66 \cdot 10^{-5}$	$2{,}83 \cdot 10^{-5}$
Velocity v_2 [m/s]	$4{,}5 \cdot 10^{-5}$	$4{,}5 \cdot 10^{-5}$

3.3 Calibration of analytical model parameters

The calibration procedure for the analytical model (Eqs. (3) and (6)) was performed by iteratively adjusting the parameters until the calculated values of the pullout force F_P and hydrodynamic force N_H reproduced the actual behaviour observed in the physical experiments. By examining Experiments 2, 3, 4, and 5, the slope stability and timing of failure were analysed. The calibrated parameters were then incorporated into the analytical model (Eqs. (3) and (6)). According to theoretical assumptions, the slope will remain stable if the pullout force exceeds the hydrodynamic force, and vice versa.

3.3.1 Hydrodynamic force N_H and pullout force F_P

Before verifying the stability of the downstream slope, the material strength parameters were defined. An internal friction angle of φ = 37° was adopted, corresponding to typical values for well-compacted sand [25]. The soil pressure coefficient K_t (Eq. (5)) was calibrated based on Experiments 2, 3, 4, and 5, resulting in a value of K_t = 0,4. In addition, the calibration of these models provided not only the internal friction angle φ, but also the interface friction angle δ between the geotextile and soil. According to recommendations, δ is usually taken as 70 % of the soil internal friction angle φ [26]; however, the calibration yielded a slightly lower value. The selected value corresponds to 55 % of the soil internal friction angle, δ = 20,35°. Table 5 presents the calibrated parameters required to calculate the hydrodynamic force, whereas Table 6 lists the values of the elementary forces and hydrodynamic force. The calculated values of the pullout force F_P for Models 2 to 5 are shown in Table 7.

Table 5. Parameters required for calculation of hydrodynamic force N_H

Hydraulic conductivity k (m/s)	Saturated unit weight of soil γ_{sat} (kg/m^3)	Internal friction angle of soil φ (°)	Soil pressure coefficient K_t
$5 \cdot 10^{-5}$	20,2	37	0,4

Table 6. Values of elementary forces and hydrodynamic force N_H

Force (N)	h_{an} = 10 cm (Models 2, 3, and 6)	h_{an} = 20 cm (Models 4, 5, and 7)
F_1	2,1	8,5
P_1	5,1	20,4
I_1	$3{,}30 \cdot 10^{-8}$	$1{,}67 \cdot 10^{-8}$
I_2	$2{,}65 \cdot 10^{-8}$	$2{,}65 \cdot 10^{-8}$
N_H	7,2	28.9

3.3.2 Stability evaluation

The calculated force magnitudes and their corresponding lever arms were used to determine the moment about Point A. According to Table 7, for a wrap-around height of h_{an} = 10 cm, the

moment M_A was negative for Model 2, leading to slope instability. For Model 3, the analytical calculation yielded $M_A \approx 0$. This indicates that an anchorage length L_{an} of 6 cm represents the stability limit under ideal analytical conditions. In the models with h_{an} = 20 cm, the moment M_A was negative for Model 4 and positive for Model 5. The results of the analytical models were in good agreement with those of the physical experiments (Table 7).

Table 7. Moment M_A and stability evaluation for Models 2, 3, 4, and 5

Variant	Moment M_A	Evaluation	Physical experiment
Model 2	F_P = 1,3 N; N_H = 7,2 N; M_A = −0,12 Nm	Unstable slope	Unstable
Model 3	F_P = 2,8 N; N_H = 7,2 N; M_A = 0,03 Nm	Limit state of stability	Unstable
Model 4	F_P = 4,5 N; N_H = 28,9 N; M_A = −0,93 Nm	Unstable slope	Unstable
Model 5	F_P = 15,3 N; N_H = 28,9 N; M_A = 1,13 Nm	Stable slope	Stable

3.3.3 Numerical simulation

Finally, a numerical simulation of the slope stability was performed using SLOPE/W. The effect of the pullout force F_P was considered based on the surcharge loads. The unit weights of the surcharge load γ_S required to define the surcharge load were derived directly from the calculated pullout forces FP for each model (Eq. (8)). In this manner, the additional resistance provided by the geotextile was successfully simulated, and the obtained safety factors confirmed the results presented in Table 7. When determining the critical slip surface, the time corresponding to the failure observed in the respective physical experiments was considered. Figure 6 shows the critical slip surfaces for numerical models 1 to 5. For Model 1, the factor of safety FS was determined for the slip surface that best matched that observed in Experiment 1. The factor of safety for this slip surface at the time of failure was F_S = 0.433, clearly indicating the instability of the downstream slope. For Models 2 and 3, the numerical simulation produced F_S = 0,646 and F_S = 0,988, respectively, confirming the instability observed i Experiments 2 and 3. Because the F_S value for Model 3 was close to 1, the anchorage length of L_{an} = 6 cm can be considered as the limit length for ensuring slope stability. Thus, the numerical model supported the analytical assessment. Numerical model 4 confirmed the instability (F_S = 0,646) observed in the physical experiment and estimated using the analytical approach. For Model 5, F_S = 1,204 was obtained, confirming the slope stability demonstrated in both the experiment and Model 5.

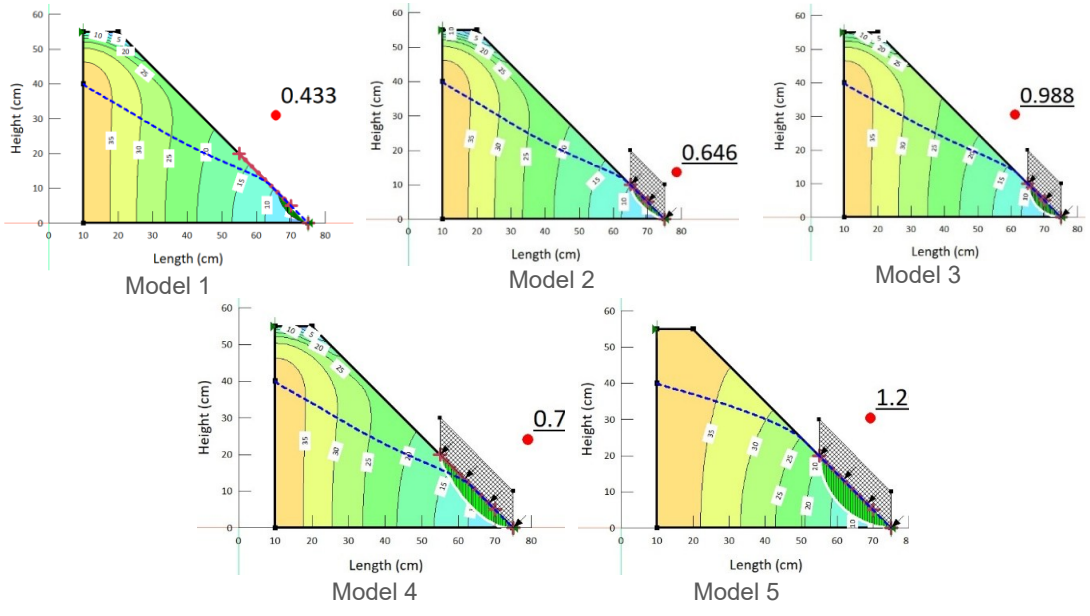

Figure 6. Critical slip surface and factor of safety FS for numerical models 1 to 5

3.4 Model validation

The validation of the analytical model through comparison with the numerical model and physical experiments was performed in the following sequence:

- Analytical calculation: Using the calibrated values, the hydrodynamic and pullout forces were calculated for two new cases, Models 6 and 7.
- Numerical simulation: The unit weight of the surcharge load γ_S was computed and subsequently applied in the numerical analysis,
- Physical experiment: Based on the results of the analytical and numerical models, the expected behaviour of the physical model was hypothesised and verified by constructing a model in the laboratory.

3.4.1 Analytical calculation

The calculation was performed for two new models: Model 6 (h_{an} = 10 cm, L_{an} = 8 cm) and Model 7 (h_{an} = 20 cm, L_{an} = 12 cm). The results of the analytical calculations for Models 6 and 7 are listed in Table 8. Based on these results, it was expected that Models 6 and 7 would remain stable during the physical experiments. Furthermore, as the difference between F_I and N_H in Model 7 was relatively small, the factor of safety in the numerical simulation was expected to be approximately $F_S \approx 1$.

Table 8. Results of analytical calculation for Models 6 and 7

Parameter	Model 6	Model 7
h_{an} (cm)	10,00	20,00
L_{an} (cm)	8,00	12,00
N_H (N)	7,20	28,90
F_P (N)	5,00	11,20
M_A (Nm)	0,25	0,31

3.4.2 Numerical simulation

The results of the numerical simulations are shown in Figure 7. Factors of safety $F_S > 1$ were obtained, confirming the stability of the slope for both models. The factor of safety for Model 7 was close to the limit value of $F_S \approx 1$, which is consistent with the previously presented interpretation of the analytical results.

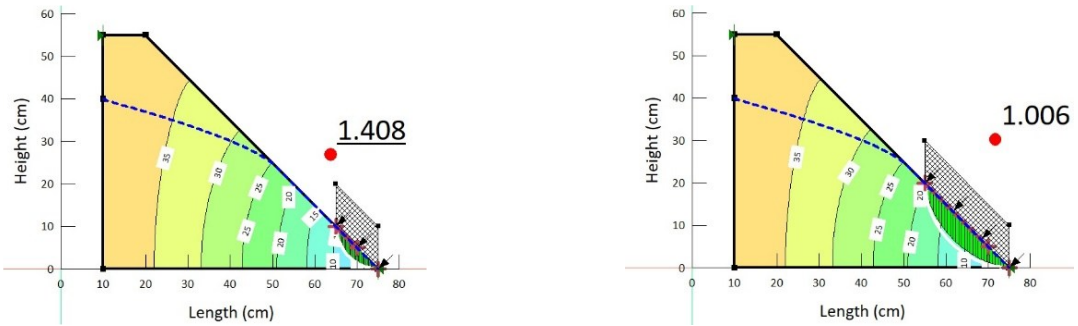

Model 6 Model 7

Figure 7. Numerical simulation of validation models

3.4.3 Physical experiments: Models 6 and 7

In Models 6 and 7, no shear failure of the slope occurred, which is consistent with both the analytical calculations and numerical simulations. This confirms that the adopted anchorage lengths, L_{an} = 8 cm (Model 6) and L_{an} = 12 cm (Model 7), were sufficient to ensure slope stability. However, in Model 6, 304 s after saturation, external erosion was observed above the

geotextile (Figure 8a). The erosion manifested as the washing out of finer soil particles owing to the action of the hydrodynamic force. The numerical simulation of Model 6 in SEEP/W indicated an exit hydraulic gradient of i = 0,6. The exit hydraulic gradient was obtained directly from the numerical seepage analysis of the finite element cell corresponding to the location where erosion occurred in the physical experiment. Considering that the reference value of the critical hydraulic gradient for this type of sand is i_{cr} = 0,12 [27], it can be concluded that the local failure was not caused by an insufficient anchorage length of the geotextile, but rather, by exceeding the critical gradient.
This case highlights the fact that numerical models are useful tools, but their results must be validated through physical observations and engineering judgment. Figure 8b shows the results of Experiment 7 at full saturation, where slight bulging of the geotextile was observed owing to the action of hydrodynamic forces and soil displacement.

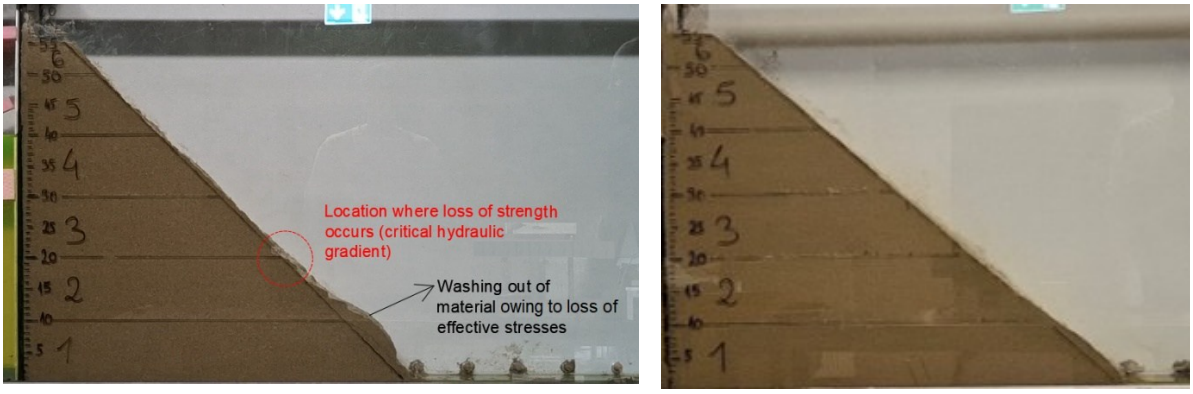

a) b)

Figure 8. Physical modelling: a) Experiment 6; and b) Experiment 7

3.5 Stability forecast

To evaluate the influence of the model geometry on stability, analytical and numerical analyses were performed for embankment models with downstream slope gradients of 1:1.5 (Models 8 and 9) and 1:2 (Models 10 and 11). The analyses were performed for both wrap-around heights, h_{an} = 10 and 20 cm. The calibrated parameters obtained from the previous models were adopted. The objective was to determine the critical anchorage length, that is the length above which the stability of the embankment was ensured (the minimum length required to produce a positive moment about Point A). The results are presented in Table 9. The critical anchorage length for Models 8 and 10 (h_{an} = 10 cm) was L_{an} = 8 cm. The increase in the anchorage length Lan related to Model 3 was attributed to the reduction in soil weight above the geotextile. The critical anchorage lengths for Models 9 and 11 (h_{an} = 20 cm) were L_{an} = 14 and 16 cm, respectively. The factors of safety obtained from the numerical analysis were approximately F_S = 1. Thus, the critical anchorage lengths predicted by the analytical model agreed well with the numerical stability evaluation.

Table 9. Values of forces from analytical model and numerical simulation

Variant	Analytical model	Numerical model Critical slip surface and factor of safety
Model 8 1:1,5 h_{an} = 10 cm L_{an} = 8 cm	N_H = 7,2 N F_P = 3,3 N M_A = 0,09 Nm	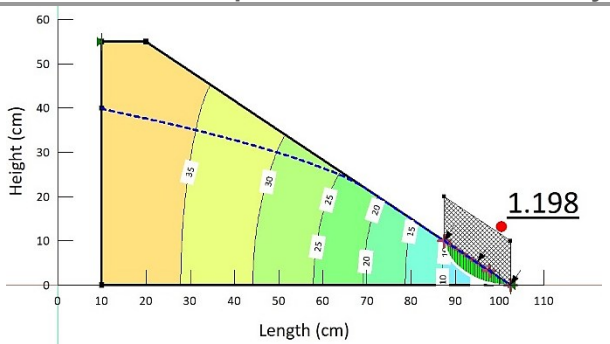
Model 9 1:1,5 h_{an} = 20 cm L_{an} = 14 cm	N_H = 28,9 N F_P = 10,2 N M_A = 0,11 Nm	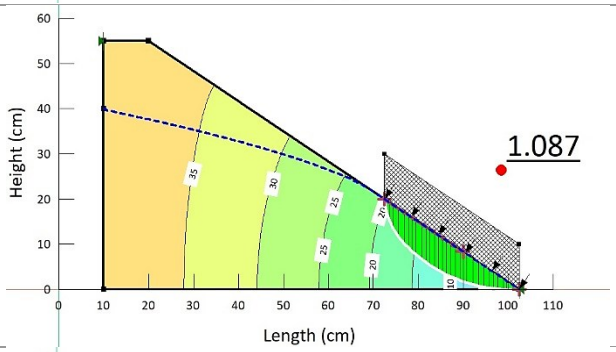
Model 10 1:2 h_{an} = 10 cm L_{an} = 8 cm	N_H = 7,2 N F_P = 2,5 N M_A = 0,01 Nm	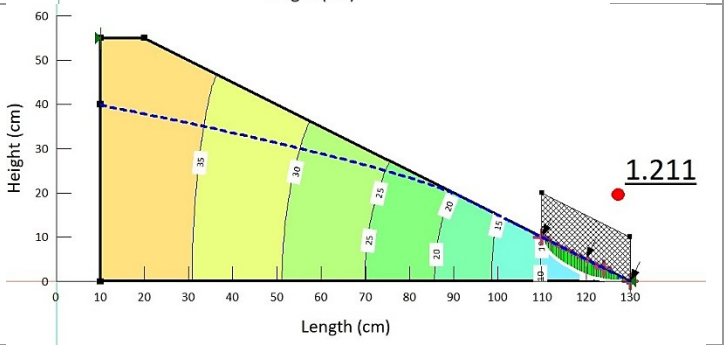
Model 11 1:2 h_{an} = 20 cm L_{an} = 16 cm	N_H = 28,9 N F_P = 9,9 N M_A = 0,07 Nm	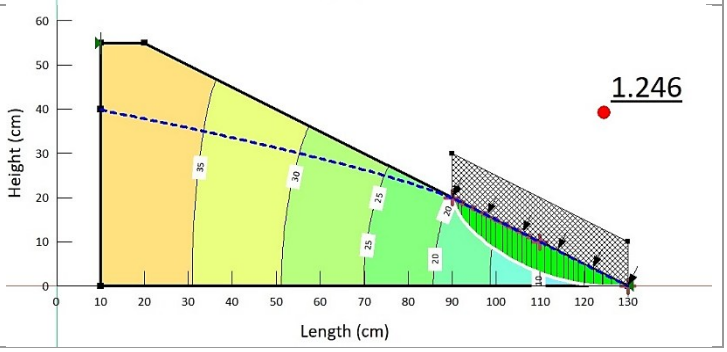

4 Conclusion

This study explored an alternative method for representing the influence of geotextile wrap-around and anchorage in numerical stability analyses. The main contribution of this study is the development of an analytical framework that enables a simplified assessment of the effects of geotextile pullout on the local slope stability, primarily at the conceptual level.

Calibration and validation performed using physical models indicated satisfactory agreement between the analytical predictions, numerical simulations, and experimental observations. The results suggest that the calibrated parameters can be applied to different geotextile

configurations at the same slope inclination while maintaining consistency in the predicted stability response. The analytical model was also examined for embankments with different downstream slope inclinations. The observed agreement with the numerical results indicates that the proposed formulation retains coherence across varying geometries within the limits of the adopted assumptions and experimental scale.

The combined use of physical experiments, analytical modelling, and numerical simulations proved effective in improving the understanding of local instability mechanisms in geotextile-reinforced slopes. This integrated approach allowed for cross-verification of the results and provided insight into the interaction between seepage, geotextile behaviour, and slope stability. Despite the encouraging agreement, the proposed methodology is subject to limitations arising from simplified analytical assumptions and the small scale of the physical models. Consequently, the analytical model should be regarded as an exploratory and supportive tool rather than a direct design method. Further investigation at larger scales and under broader conditions is required before extending its application to practical engineering design.

References

[1] Koerner, R. M. *Designing with Geosynthetics*. 6th Edition, Volume I. USA: Xlibris Corporation, 2012.

[2] Federal Emergency Management Agency. Geotextiles in Embankment Dams - Status Report on the Use of Geotextiles in Embankment Dam Construction and Rehabilitation. Accessed: June 11, 2026. Available at: https://damsafety.org/content/geotextiles-embankment-dams-status-report-use-geotextiles-embankment-dam

[3] Shukla, S. K.; Yin, J. H. *Fundamentals of geosynthetic engineering. in Proceedings and monographs in engineering, water and earth sciences*. London; New York: Taylor & Francis/Balkema, 2006.

[4] Cazzuffi, D.; Giroud, J. P.; Scuero, A.; Vaschetti, G. Geosynthetic barriers systems for dams. In: *9th International Conference on Geosynthetics - 9ICG*. May 22-28, 2010, Guaruja, Brazil, IGS, ABMS; 2010.

[5] Koerner, R. M.; Koerner, G. R. An extended data base and recommendations regarding 320 failed geosynthetic reinforced mechanically stabilized earth (MSE) walls. *Geotextiles and Geomembranes*, 2018, 46 (6), pp. 904-912. https://doi.org/10.1016/j.geotexmem.2018.07.013

[6] Lajevardi, S. H. et al. Geosynthetics anchorage with wrap around: experimental and numerical studies. *Geosynthetics International*, 2015, 22 (4), pp. 273-287. https://doi.org/10.1680/gein.15.00010

[7] Mamat, R. C. et al. Stability assessment of embankment on soft soil improved with prefabricated vertical drains using empirical and limit equilibrium approaches. *International Journal of Advanced Trends in Computer Science and Engineering*, 2019, 8 (1.6), pp. 444-449. https://doi.org/10.30534/ijatcse/2019/6481.62019

[8] BahooToroody, F. et al. Reliability estimation of reinforced slopes to prioritize maintenance actions. *International Journal of Environmental Research and Public Health*, 2021, 18 (2), 373. https://doi.org/10.3390/ijerph18020373

[9] Šreng, Ž.; Minažek, K.; Grubišić, M.; Jelović, M. Physical and Numerical Modelling of a Geotextile Influence on Embankment Stability. *Advances in Civil and Architectural Engineering*, 2025, 16 (31), pp. 14-30. https://doi.org/10.13167/2025.31.2

[10] Giroud, J.P. Development of criteria for geotextile and granular filters. In: *9th International Conference on Geosynthetics - 9ICG*. May 22-28, 2010, Guaruja, Brazil, IGS, ABMS; 2010.

[11] Thuo, J. N.; Yang, K. H.; Huang, C. C. Infiltration into unsaturated reinforced slopes with nonwoven geotextile drains sandwiched in sand layers. *Geosynthetics International*, 2015, 22 (6), pp. 457-474. https://doi.org/10.1680/jgein.15.00026

[12] Arsyad, M. Road embankment full-scale investigation on soft soil with geotextile stabilization. *International Journal of GEOMATE*, 2020, 19 (71), pp. 145-152. https://doi.org/10.21660/2020.71.04022
[13] Rahman, M. M.; Lee, Y. D. Deformation and stability analysis of embankment foundation soil supported by dcm (deep cement mixing) columns and geotextiles. *Journal of Korean Society of Hazard Mitigation*, 2012, 12 (3), pp. 93-100. https://doi.org/10.9798/kosham.2012.12.3.093
[14] Zimbu, S. A.; Thuo, J.; Ambassah, N. Evaluation of the performance of reinforced red coffee soils embankments subject to rainfall event. *Civil Engineering Journal*, 2018, 4 (11), pp. 2548-2559. https://doi.org/10.28991/cej-03091180
[15] El Hourani, D. W.; Nwaogazie, I. L.; TomJaja, G. W. Finite element modeling of geotextilereinforced embankments on soft clay. *Open Journal of Civil Engineering*, 2023, 13 (1), pp. 48-57. https://doi.org/10.4236/ojce.2023.131004
[16] Šreng, Ž.; Kaluđer, J.; Šperac, M.; Miličević, S. I. Visualization and analysis of seepage below the dam foundation. *Environmental Engineering - Inženjerstvo okoliša*, 2023, 10 (1-2), pp. 1-11. https://doi.org/10.37023/ee.10.1-2.1
[17] U.S. Department of Transportation, Federal Highway Administration. *Mechanically Stabilized Earth Walls and Reinforced Soil Slopes Design and Construction Guidelines*. USA: FHWA-NHI-00-043; 2001.
[18] Geo-Slope Internatioal Ltd., Seepage Modeling with SEEP/W: An Engineering Methodology. Accessed: June 11, 2026. Available at: https://ottegroup.com/wp-content/uploads/2021/02/seep-modeling-June2015.pdf
[19] Zhang, H. et al. Soil–water characteristic curves of extracellular polymeric substances-affected soils and sensitivity analyses of correlated parameters. *Water Supply*, 2021, 21 (3), pp. 1323-1333. https://doi.org/10.2166/ws.2020.377
[20] Arafat, A.; Al-Omran, A. Evaluating the Effects of Biochar and SAP Polymer on Soil Physical Quality Indices. *Communications in Soil Science and Plant Analysis*, 2020, 51 (8), pp. 1123-1135. https://doi.org/10.1080/00103624.2020.1751193
[21] Datta, S.; Taghvaeian, S.; Stivers, J. Understanding Soil Water Content and Thresholds for Irrigation Management. *Oklahoma Cooperative Extension Service*, 2017. https://doi.org/10.13140/RG.2.2.35535.89765
[22] Look, B. *Hanbook of geotechnical investigation and design tables*. London: Taylor and Francis Group, 2007.
[23] Das, B.; Sobhan, K. *Principles of Geotechnical Engineering*. 9th Edition, USA: Cengage Learning, 2018.
[24] Craig, R.F. *Craig's Soil Mechanics*. 7th Edition, UK: CRC Press, 2004. https://doi.org/10.4324/9780203494103
[25] Prakash, K.; Sridharan, A.; Manoj, M. N. Friction Angles of Sands: An Appraisal. *Geotechnical and Geological Engineering*, 2023, 41, pp. 4865-4872. https://doi.org/10.21203/rs.3.rs-2650302/v1
[26] Mulabdić, M.; Kaluđer, J.; Minažek, K.; Matijević, J. *Priručnik za primjenu geosintetika u nasipima za obranu od poplava*. Osijek: Sveučilište Josipa Jurja Strossmayera u Osijeku, Građevinski fakultet Osijek, 2016. [in Croatian]
[27] Savić, Lj. *Uvod u hidrotehničke građevine*. 3rd Edition, Beograd: Građevinski fakultet Beograd, 2022. [in Serbian]